# AFRL-PR-WP-TP-2007-208

# AIRCRAFT THERMAL MANAGEMENT USING LOOP HEAT PIPES: EXPERIMENTAL SIMULATION OF HIGH ACCELERATION ENVIRONMENTS USING THE CENTRIFUGE TABLE TEST BED (POSTPRINT)

**Andrew J. Fleming, Quinn H. Leland, Kirk L. Yerkes, Levi J. Elston and Scott K. Thomas**

**NOVEMBER 2006**

**Approved for public release; distribution unlimited.**

**STINFO COPY**



**PROPULSION DIRECTORATE**
**AIR FORCE MATERIEL COMMAND**
**AIR FORCE RESEARCH LABORATORY**
**WRIGHT-PATTERSON AIR FORCE BASE, OH 45433-7251**

# REPORT DOCUMENTATION PAGE

*Form Approved*
*OMB No. 0704-0188*



| 1. REPORT DATE *(DD-MM-YY)* | 2. REPORT TYPE | 3. DATES COVERED *(From - To)* |
|---|---|---|
| November 2006 | Conference Paper Postprint | 08/01/2004 – 09/01/2006 |

**4. TITLE AND SUBTITLE**
AIRCRAFT THERMAL MANAGEMENT USING LOOP HEAT PIPES: EXPERIMENTAL SIMULATION OF HIGH ACCELERATION ENVIRONMENTS USING THE CENTRIFUGE TABLE TEST BED (POSTPRINT)

**5a. CONTRACT NUMBER**
In-house

**5b. GRANT NUMBER**

**5c. PROGRAM ELEMENT NUMBER**
N/A

**6. AUTHOR(S)**
Andrew J. Fleming, Quinn H. Leland, Kirk L. Yerkes, and Levi J. Elston (AFRL/PRPS)
Scott K. Thomas (Wright State University)

**5d. PROJECT NUMBER**
3145

**5e. TASK NUMBER**
20

**5f. WORK UNIT NUMBER**
C9

**7. PERFORMING ORGANIZATION NAME(S) AND ADDRESS(ES)**
Electrochemistry and Thermal Sciences Branch (AFRL/PRPS)
Power Division
Propulsion Directorate
Air Force Research Laboratory, Air Force Materiel Command
Wright-Patterson Air Force Base, OH 45433-7251

Wright State University
Dayton, OH 45435

**8. PERFORMING ORGANIZATION REPORT NUMBER**
AFRL-PR-WP-TP-2007-208

**9. SPONSORING/MONITORING AGENCY NAME(S) AND ADDRESS(ES)**
Propulsion Directorate
Air Force Research Laboratory
Air Force Materiel Command
Wright-Patterson AFB, OH 45433-7251

**10. SPONSORING/MONITORING AGENCY ACRONYM(S)**
AFRL-PR-WP

**11. SPONSORING/MONITORING AGENCY REPORT NUMBER(S)**
AFRL-PR-WP-TP-2007-208

**12. DISTRIBUTION/AVAILABILITY STATEMENT**
Approved for public release; distribution unlimited.

**13. SUPPLEMENTARY NOTES**
Conference paper published in the Proceedings of the 2006 SAE Power Systems Conference, published by SAE International. 

PAO Case Number: AFRL/WS 06-2611; Date cleared: 06 Nov 2006. Paper contains color.

**14. ABSTRACT**
The objective of this paper is to describe the design of an experiment that will examine the effects of elevated acceleration environments on a high-temperature, titanium-water loop heat pipe for actuator cooling. An experimental test setup has been designed for mounting a loop heat pipe on an 8-ft-diameter centrifuge table, which is capable of radial accelerations of up to 12-g's. A high-temperature PAO loop will interface the condenser of the loop heat pipe to simulate the rejection of the transported heat to an elevated temperature. In addition to LHP experimentation, a mathematical model has been developed for aerodynamic heating of high-speed aircraft. A flat plate at zero-incidence, used to model an aircraft wing, was subjected to sub- and supersonic flow to examine whether heat will be rejected or absorbed. The results of this analysis will be used to determine the condenser conditions of the loop heat pipe during centrifuge testing.

**15. SUBJECT TERMS**
Loop heat pipe, varying acceleration, LHP, aerodynamic heating, actuator cooling, centrifuge table

| 16. SECURITY CLASSIFICATION OF: | | | 17. LIMITATION OF ABSTRACT: | 18. NUMBER OF PAGES | 19a. NAME OF RESPONSIBLE PERSON (Monitor) |
|---|---|---|---|---|---|
| a. REPORT | b. ABSTRACT | c. THIS PAGE | | | Andrew J. Fleming |
| Unclassified | Unclassified | Unclassified | SAR | 16 | 19b. TELEPHONE NUMBER *(Include Area Code)* N/A |

**Standard Form 298 (Rev. 8-98)**
Prescribed by ANSI Std. Z39-18

# Aircraft Thermal Management Using Loop Heat Pipes: Experimental Simulation of High Acceleration Environments Using the Centrifuge Table Test Bed

**Andrew J. Fleming, Quinn H. Leland, Kirk L. Yerkes, Levi J. Elston**
Air Force Research Laboratory, Wright-Patterson Air Force Base, Ohio, 45433

**Scott K. Thomas**
Wright State University, Dayton, Ohio, 45435



## ABSTRACT

The objective of this paper is to describe the design of an experiment that will examine the effects of elevated acceleration environments on a high-temperature, titanium-water loop heat pipe for actuator cooling. An experimental test setup has been designed for mounting a loop heat pipe on an 8-ft-diameter centrifuge table, which is capable of radial accelerations of up to 12-g's. A high-temperature PAO loop will interface the condenser of the loop heat pipe to simulate the rejection of the transported heat to an elevated temperature. In addition to LHP experimentation, a mathematical model has been developed for aerodynamic heating of high-speed aircraft. A flat plate at zero-incidence, used to model an aircraft wing, was subjected to sub- and supersonic flow to examine whether heat will be rejected or absorbed. The results of this analysis will be used to determine the condenser conditions of the loop heat pipe during centrifuge testing.

## INTRODUCTION

The More Electric Aircraft initiative (MEA) is the concept for future aircraft including warfighter, transport, helicopters, and commercial aircraft [1]. The MEA initiative has improved aircraft reliability, maintainability, support, and operations cost as well as reduce weight, volume, and enhance battle damage reconfigurability [2]. This approach has been adopted by the United States Air Force since the early 1990's with the purpose of reducing or removing as many of the hydraulic, mechanical, and pneumatic power systems and replacing them with electrically driven devices. This approach to aircraft design was first envisioned during World War II. However, at that time, the power generation capability and power conditioning equipment required was not feasible due to volume requirements. As a result, hydraulic, pneumatic, and mechanical systems became the norm for aircraft until this initiative.

While the reduction of hydraulic, pneumatic, and mechanical systems in favor of electrical systems is a favorable route, it presents a problem in terms of thermal management. Removing the centralized hydraulic system with an electrical based system removes a primary method of transporting and removing waste heat [3]. With the MEA approach, heat loads become localized. This means taking individual components in the aircraft and locally handling their heat rejection.

The MEA initiative has resulted in the development of high-temperature, high-efficiency, and high-density power electronic component technologies. The next-generation power electronics will operate at cold plate temperatures of up to 200ºC, which presents an opportunity to reject heat through the aircraft skin to the ambient using passive cooling. The operating envelope for military aircraft places stringent requirements on any proposed thermal management system. The on-board electrical flight control actuation system operates at altitudes from sea level to above 40 kft, airspeeds from stationary to supersonic speeds, transient body forces up to 9-g due to maneuvering, and ambient temperatures from -80 to 45ºC. Possible thermal management scenarios include a direct connection of the electronics package to the skin or the use of a loop heat pipe between the package and the skin to provide mounting flexibility. As a result, it is important to understand loop heat pipe operation and the effects of acceleration on loop heat pipe performance.

The loop heat pipe (LHP) was invented in the early 1980's by Maidanik in the former Soviet Union. This device was patented in the United States in 1985 [4]. The operation of a LHP is quite simple. LHPs are two-phase thermal transport devices that operate passively. They use the latent heat of vaporization to transport heat from one location to another. The LHP consists of an evaporator, compensation chamber, wick, liquid and vapor transport lines, and a condenser as shown in Figure 1.

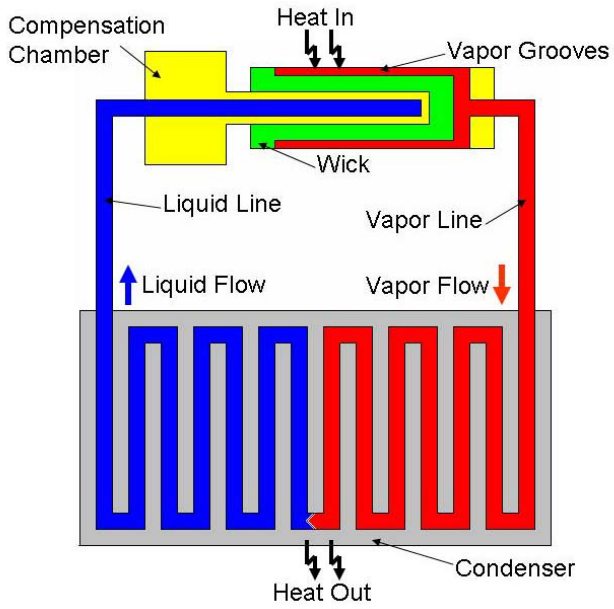


**Figure 1. Basic LHP schematic.**

Heat is applied at the evaporator. The working fluid of the LHP is circulated inside the evaporator via the wick until it becomes superheated vapor. The vapor is captured in the grooves and is directed to the vapor line due to the pressure differential between the evaporator and condenser. A meniscus is developed in the wick and establishes a capillary head which prevents vapor from traveling backwards away from the vapor transport lines. The vapor continues to the condenser where a cold plate is attached to remove the heat and condense the vapor to a liquid. The liquid then continues to the liquid transport line at the exit of the condenser and then to the compensation chamber, which acts a reservoir for the system [5].

Ku et al. [6] performed experiments on a miniature LHP with varying acceleration forces created by use of a spin table to examine the effects on start-up. Several different tests were conducted, including LHP startup before acceleration force applied and vice versa, as well as varying heat load inputs. Periodic inputs of acceleration forces were also tested. The centrifugal accelerations varied from 1.2 g's to 4.8 g's. Their tests indicate that the superheat in the evaporator appeared to be independent of input heat load as well as acceleration force. When temperature overshoot was examined, for heat loads greater than 50 W, there was essentially no overshoot. For smaller heat loads, such as at 5 W, a temperature overshoot by a few degrees was always observed, but for 25 W, the temperature overshoot ranged from 0°C to 45°C. In every test, the LHP started successfully.

Ku et al. [7], in an extension of the previous experimental study, further examined the temperature stability of the same miniature LHP under varying heat loads and acceleration forces. Their results show that the body force due to acceleration causes a redistribution of fluid in the evaporator, condenser, and compensation chamber. This in turn changed the LHP operating temperature. The effect was not universal, in the sense that all the operating conditions need to be taken into account. With sufficient time, constant acceleration could either increase or decrease the LHP operating temperature. Periodic acceleration lead to a quasi-steady operating temperature. Temperature hysteresis could also be caused by acceleration forces on a LHP. Throughout testing the LHP continued operate without problems.

Kaya et al. [8] conducted more testing on a small loop heat pipe subjected to varying acceleration forces. Testing was conducted between 1.2 and 4.8g. Their results show that accelerating forces creates another pressure drop and changes how the working fluid is dispersed in the LHP. The fluid disbursement in the LHP affected the boiling and temperature overshoot in an random manner. This in turn affects the startup characteristics and LHP operating temperature.

The objective of this paper is to describe an experiment that will be used to determine the effects of elevated acceleration fields on a titanium-water loop heat pipe. The effective heat transfer coefficient of the evaporator and condenser, as well as thermal resistance and steady state maximum heat input will be examined with respect to radial acceleration. Previous research in this area was limited to radial acceleration of 4.8 g's. This experimentation will be conducted up to 10 g's, with heat loads up to 750 W. This report documents the status of the experimental design and the proposed method of gathering and reducing the experimental data. In addition, this paper will also present a mathematical model of aerodynamic heating for high-speed aircraft.

## EXPERIMENTAL SETUP

The purpose of the experiment is to examine a titanium-water loop heat pipe performance in an elevated body-force environment for steady-state and transient response using a centrifuge table located at the Air Force Research Laboratory located at Wright-Patterson AFB (AFRL/PRPS). The LHP is being manufactured by Advanced Cooling Technologies (ACT) of Lancaster, PA. Design requirements specified by AFRL/PRPS are shown in Table 1.

Specifically, AFRL/PRPS was interested in maximizing the heat load and heat flux capabilities for this loop heat pipe. Also, the transport lines were requested to be serpentine rather than coiled. This will reduce the acceleration gradient across the loop heat to provide more realistic results.

After analysis and design, ACT determined the parameters of the LHP show in Table 2.

**Table 1. AFRL/PRPS design requirements.**

| Requirement | Parameter |
|---|---|
| Thermal | |
| Heat Load | 500 W up to 5000 W |
| Heat Flux | 3 W/cm$^2$ up to 30 W/cm$^2$ |
| Operating Temperature | 200°C |
| Condenser Heat Sink Temperature | 5 to 140°C |
| Tilt in One G | ± 0 inches, horizontal |
| Conductance | 50°C/W |
| Proof of Pressure Test | 450 psi (200°C) |
| Materials | |
| Evaporator Envelope Material | Titanium, CP Grade 2 |
| Evaporator Wick Material | Titanium, CP Grade 2 |
| Transport Line Material | Titanium, CP Grade 2 |
| Working Fluid | Water |
| LHP Dimensions | |
| Evaporator Configuration | 1.0" OD up to 10" Long |
| Evaporator Footprint | 8" x 4" |
| Condenser Footprint | 12" x 11.25" |
| Transport Line Lengths | Approx. 96" |

**Table 2. ACT LHP geometric design parameters.**

| Transport Lines | |
|---|---|
| Vapor Line Length | Approx. 96" |
| Vapor Line Diameter | .375" OD x .035" wall |
| Liquid Line Length | Approx. 132" |
| Liquid Line Diameter | .25" OD x .035" wall |
| Condenser Line Length | Approx.110" |
| Condenser Line Diameter | .375" x .035" wall |
| Compensation Chamber | |
| Diameter | 2.375" OD |
| Length | 4.5" |
| Chamber Location | CL with evaporator |
| Wick Properties | |
| Effective Radius | 9.1μm |
| Permeability | 1.2x10$^{-12}$ m$^2$ |
| Outside Diameter | 0.900" |
| Length | 8" |
| Inside Diameter | 0.315" |
| Grooves | 6 |
| Groove Depth | 0.060" |
| Groove Width | 0.060" |

Figure 2 shows the LHP design by ACT. Note the serpentine transport lines of the LHP.

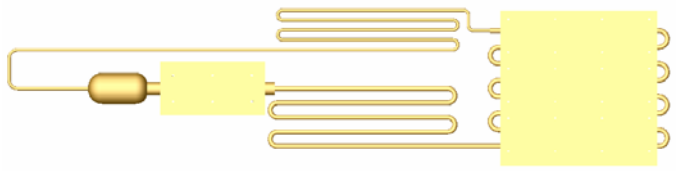

**Figure 2. ACT LHP design.**

The 8-foot-diameter horizontal centrifuge table is driven by a 20-hp dc motor. The centrifuge table is shown in Figure 3.

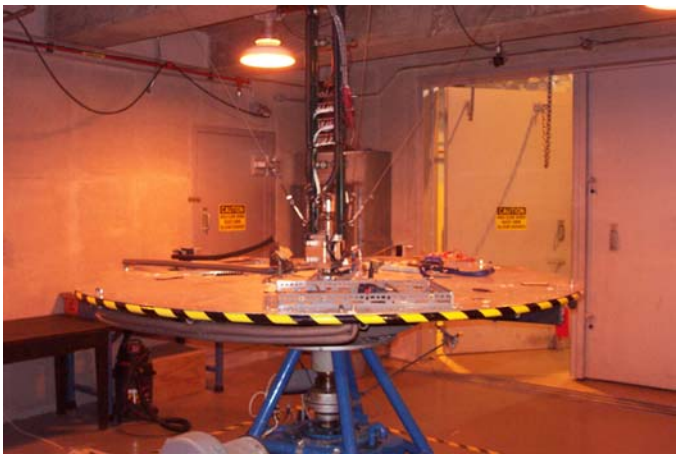

**Figure 3. AFRL/PRPS centrifuge table.**

The acceleration field near the loop heat pipe is measured by a triaxial accelerometer. The acceleration gradient across the LHP will be determined as a percentage of the difference between the inner and outer radius and can be calculated from the readings of the accelerometer using a coordinate transformation.

Power is supplied to the Minco mica heater on the evaporator by a precision power supply (Kepco ATE150-7m) through power slip rings to the table. These slip rings were separated from the instrumentation slip rings to reduce induced electrical noise. While the current reading can be made directly using a precision ammeter, the voltage across the mica heater must be measured on the rotating table using the instrumentation slip rings because of the voltage drop between the control room and the table.

Heat from the condenser is rejected by using a series of three Lytron cold plates connected to a high temperature polyalphaolefin (PAO) fluid loop. Figure 4 shows a schematic diagram of this fluid loop.

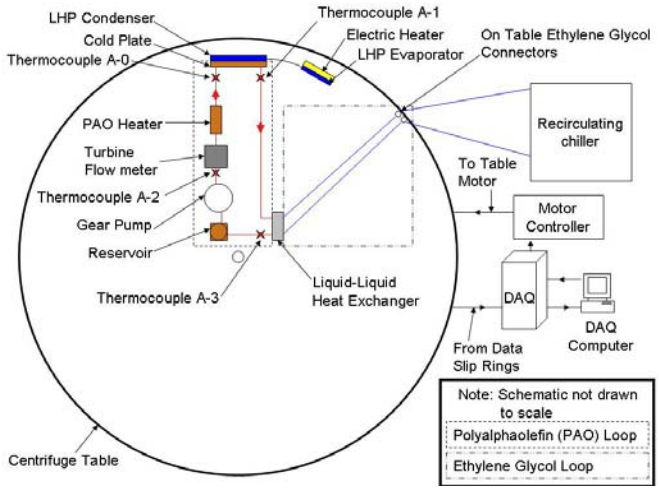


**Figure 4. High temperature fluid loop schematic.**

Heat is rejected from this fluid loop by a liquid-liquid heat exchanger using an ethylene-glycol/water mixture that is delivered to the rotating centrifuge table via a double-pass hydraulic rotary coupling (Deublin). The temperature of the coolant is maintained at a constant setting by a recirculating chiller (Neslab HX-300). The mass flow rate of the coolant mixture is controlled using a high-pressure booster pump, which aids the low-pressure pump in the recirculating chiller.

Data from the loop heat pipe experiment are acquired through the custom-built forty-channel instrumentation slip ring, using a data acquisition system. Temperatures, pressures, mass flow rates, accelerations, voltages and amperages are all measured using a data acquisition mainframe (Agilent VXI E8408A) with a command module (Agilent E1406A), 5 ½ digit multimeter module (Agilent E1411B), and a 64-channel 3-wire multiplexer module (Agilent E1476A). In addition, the mass flow rate of the high temperature fluid loop PAO, the rotational speed of the centrifuge table, and the heater power are controlled using a 8/16-channel D/A converter module (Agilent E1418A) coupled with a custom-designed LabVIEW virtual instrument. Communication between the data acquisition unit and the computer is established using a general purpose interface bus (GPIB).

Gathering temperature data from rotating machinery using slip rings presents unique problems. Firstly, when the thermocouple wires are connected to the wires leading to a slip ring, at least one extra junction is created, depending on the materials of the thermocouple wires. To avoid this problem, a Type E thermocouple amplifier was installed on the centrifuge table. This converts the millivoltage signals from the thermocouples to 0 to 10 volt signals without the creation of extra junctions. Another problem that is present when slip rings are used is electrical noise. This problem was reduced (not eliminated) by the use of a low-pass filter for each of the thermocouple signals coming from the table before the data acquisition system.

The LHP will be mounted vertically and curved to match the radial profile. A tri-axial accelerometer is mounted to the table with a coordinate transformation used to measure the acceleration field across the LHP. Two stands made of phenolic G-7 will be made to hold the LHP. The setup will be mounted inside an 80/20 box with sheet metal sides to eliminate heat losses due to forced convection. The centerline of the evaporator/compensation chamber along with the transport lines and condenser will be at 101.6 cm. With the LHP evaporator/compensation chamber length, the $\Delta r\%$ will be 7.6%.

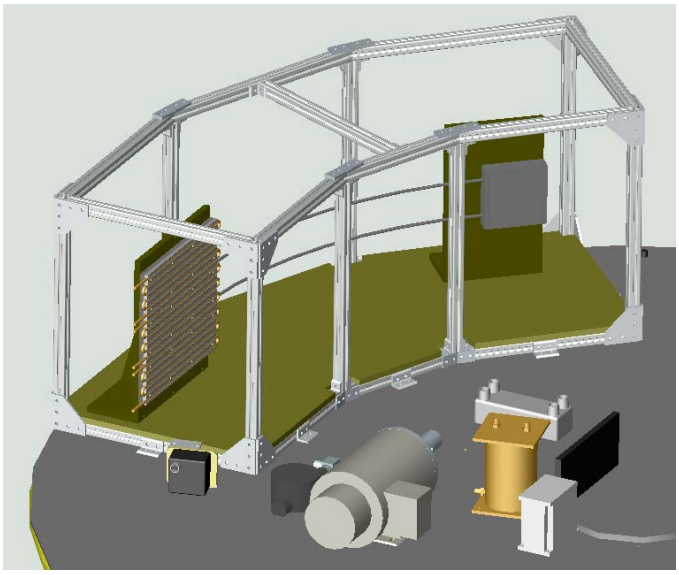

**Figure 5. Experimental setup of LHP on centrifuge table.**

## EXPERIMENT CALIBRATIONS

Thorough calibrations are required to minimize the uncertainty associated with the data collected. Two locations where this error will be minimized is with the thermocouples and high temperature fluid loop flow meter.

The thermocouples were calibrated using a Hart Scientific 6330 Calibration Bath and a Hart Scientific 1502A resistive temperature detector (RTD) capable of producing steady state temperatures of up to 280°C. The RTD has an uncertainty of ±0.009°C. The calibration bath uses Dow Corning 200.50 silicon oil. A LabVIEW program was written to interface with the data acquisition system, calibration bath, and RTD. The program incremented then decremented the bath temperature by 5°C from 40 to 230°C while providing RTD and thermocouple values. At each temperature setting, the RTD was allowed to reach steady state, which was defined by the standard deviation of the previous 100 RTD, taken at a rate of once every five seconds, dropping below 0.005°C. Then the program would read 100 more RTD and thermocouples values,

taken at a rate of once every second, average each RTD and thermocouple value set, and record them to a data file. To calibrate the thermocouples over the range of 20 to 40°C, a separate calibration bath (Brinkmann Lauda RCS 20-D) was used with manual control of the bath temperature. The bath fluid was polyalphaolefin. All of this data was compiled into one data set. Plots of RTD versus each thermocouple were generated and fifth-order polynomials were fit to each plot. The four calorimetry thermocouples in the high temperature fluid loop were calibrated over 20 to 145°C while the twelve thermocouples on the LHP were calibrated over the range of 20 to 230°C. This was done to reduce the error associated with the calorimetry of the cold plate. The overall uncertainties of the thermocouples were estimated by adding the error of the RTD, the maximum standard deviation of the 100 RTD readings, and the maximum deviation of the corrected thermocouple value from the experimental RTD average. The largest error for the high temperature fluid loop thermocouples was ±0.12°C and for the LHP thermocouples ±0.34°C.

The flow meter presents a new challenge in calibration. Since the working fluid in the high temperature fluid loop is polyalphaolefin, which has a large change in density and viscosity across the temperature range of 20 to 140°C, flow rates will need to be taken with varying PAO temperature and volumetric flow rates. To achieve this, a pump will deliver PAO to the flow meter, which will then dump the PAO to a beaker sitting on a scale. In this way, the flow meter will be calibrated for mass flow rate. This will be done in 5°C increments from 20 to 70°C, as 70°C will be the highest temperature in the high temperature fluid loop. In a sense, a three-dimensional plot of flow meter voltage and temperature versus mass flow rate will be generated. Individual mass flow rates will be interpolated from this data.

EXPERIMENTAL TEST MATRIX

The test variables for this experiment include heat input to the evaporator, heat sink temperature, and the acceleration field. Table 3 shows the experimental test matrix.

**Table 3. Experimental test matrix.**

| Heat Input, Q | Radial Acceleration, $a_r$ | Bounds |
|---|---|---|
| Step Increase | Constant | 50 < Q < 750 W, 0 < $a_r$ < 10 |
| Steady State | Step Increase | 50 < Q < 750 W, 0 < $a_r$ < 10 |
| Steady State | Transient | 50 < Q < 750 W, 0 < $a_r$ < 10, 0.01-0.06 Hz |
| Transient | Transient | Q and $a_r$ TBD by previous testing, in- and out-of-phase, coupled |
| Steady State | Periodic Burst | Q and ar TBD by previous testing |

Throughout these tests the LHP will be monitored for dry-out conditions, which are defined by Wirsch [5] as:

1. Greater than 20°C increase in evaporator temperature over a 2 minute period.
2. Dramatically steeper slope for the evaporator temperature increase than for the reservoir or vapor line.
3. Condenser temperature drops to near the cold plate operating temperature.
4. Liquid line temperature approaches ambient temperature.

Results that will be examined include steady state maximum heat input with respect to radial acceleration, thermal resistance of the LHP, and effective heat transfer coefficients for the evaporator and condenser at the various input parameters.

## MATHEMATICAL MODEL OF AERODYNAMIC HEATING FOR HIGH-SPEED AIRCRAFT

The objective of this analysis is to determine the feasibility of using loop heat pipes to dissipate waste heat from power electronics to the skin of a fighter aircraft. In the past, it has been found that the boundary condition at the condenser can be a controlling factor in the overall performance of this type of thermal management scheme. Therefore, the heat transfer removed from the aircraft skin has been determined as a function of Mach number, altitude, and skin temperature by modeling the wing as a flat plate at zero-incidence. In addition, the effects of the variable properties of air have been taken into account. Heat transfer due to thermal radiation has been neglected in this analysis due to the low skin temperatures and high airspeeds. This model will determine what the operating envelope of a LHP will be with respect to varying Mach numbers.

The temperature and density of air vary considerably with altitude and also vary day-to-day depending on weather conditions. In order to be conservative in the calculation of heat transfer coefficients, data for the highest temperature recorded with a frequency-of-occurrence of 1% were used to generate equations for temperature and density versus altitude [9] as shown in Figure 6 and Figure 7.

Also presented are data for the lowest temperature recorded with a frequency-of-occurrence of 1% [9] and data for the “standard atmosphere” [10].

The film temperature was used to evaluate the air properties [11]

$$T^* = T_\infty(0.5 + 0.039\mathrm{Ma}_\infty^2) + 0.5T_w \quad (1)$$

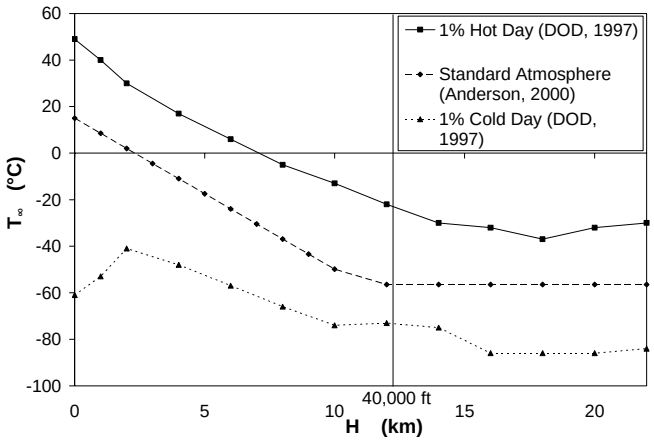


**Figure 6. Atmospheric temperature versus altitude.**

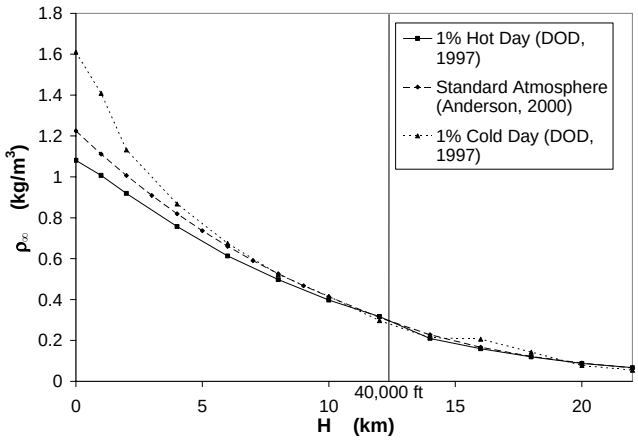


**Figure 7. Atmospheric density versus altitude.**

The air density at the film temperature and at altitude was evaluated using the perfect gas law

$$\rho^* = \rho_\infty \left( \frac{T_\infty}{T^*} \right) \tag{2}$$

The freestream speed of sound is

$$a_\infty = \sqrt{\gamma R T_\infty} \tag{3}$$

The freestream velocity is

$$U_\infty = \mathrm{Ma}_\infty a_\infty \tag{4}$$

The absolute viscosity of air is given by the following relation [12]

$$\mu = \mu_\mathrm{R} \left( \frac{T}{T_\mathrm{R}} \right)^{0.76} \tag{5}$$

where $\mu_R$ is a reference viscosity evaluated at some reference temperature $T_R$.

The Reynolds number for a plate of length L is determined by evaluating the properties of air at the freestream condition.

$$\mathrm{Re}_\mathrm{L} = \frac{\rho_\infty U_\infty L}{\mu_\infty} \tag{6}$$

Regression equations for the specific heat and Prandtl number were determined as functions of temperature using data from Incropera and DeWitt [13], as shown in Table 4.

**Table 4. Regression equations for air properties versus temperature (Incropera and DeWitt, 1990).**

| $y = a_0 + a_1 T + a_2 T^2 + a_3 T^3$, T in (K) | | | | |
|---|---|---|---|---|
| Property | $a_0$ | $a_1$ | $a_2$ | $a_3$ |
| $c_p$ (J/kg-K) | 1.0187E+03 | -6.9921E-02 | -3.3333E-05 | 4.4444E-07 |
| Pr | 8.6418E-01 | -9.4177E-04 | 1.7778E-06 | -1.2593E-09 |

The adiabatic wall temperature is [11]

$$T_\mathrm{aw} = T_\infty \left[ 1 + r \left( \frac{\gamma - 1}{2} \right) \mathrm{Ma}_\infty^2 \right] \tag{7}$$

where the recovery factor is

$$r = \begin{cases} \mathrm{Pr}^{1/2} & \text{for laminar flow} \\ \mathrm{Pr}^{1/3} & \text{for turbulent flow} \end{cases} \tag{8}$$

The local skin friction coefficient at the end of the plate is found by evaluating the air properties at the film [11].

$$C_{\mathrm{f,L}}^* = \frac{0.455}{\ln^2 \left( 0.06 \rho^* U_\infty L / \mu^* \right)} \tag{9}$$

The local Stanton number at the end of the plate is given by [11]

$$\mathrm{St}_\mathrm{L}^* = \frac{h_\mathrm{L}}{\rho^* U_\infty c_\mathrm{p}^*} = \frac{C_{\mathrm{f,L}}^* / 2}{1 + 12.7 (\mathrm{Pr}^{*2/3} - 1)(C_{\mathrm{f,L}}^* / 2)^{1/2}} \tag{10}$$

The local heat transfer coefficient at the end of the plate is

$$h_\mathrm{L} = \mathrm{St}_\mathrm{L}^* \rho^* U_\infty c_\mathrm{p}^* \tag{11}$$

The average heat transfer coefficient over the length of the plate is approximated by [11]

$$\bar{h} = 1.15 h_{\mathrm{L}} \tag{12}$$

The average heat flux dissipated over the plate is defined in terms of the adiabatic wall temperature.

$$q''_{\mathrm{w}} = \bar{h}(T_{\mathrm{w}} - T_{\mathrm{aw}}) \tag{13}$$

Three separate cases were compared using the 1% hot day data in which the altitude was $H$ = 0, 5000, and 40,000 ft and the Mach number was $\mathrm{Ma}_\infty$ = 0.98 and 1.4. For all cases, the plate length was $L$ = 1.0 m and the temperature of the plate was $T_{\mathrm{w}}$ = 135 °C. The results of the comparison are excellent with a maximum difference for the average heat transfer coefficient of less than 2%.

The adiabatic wall temperature is shown in Figure 8 as a function of altitude and Mach number.

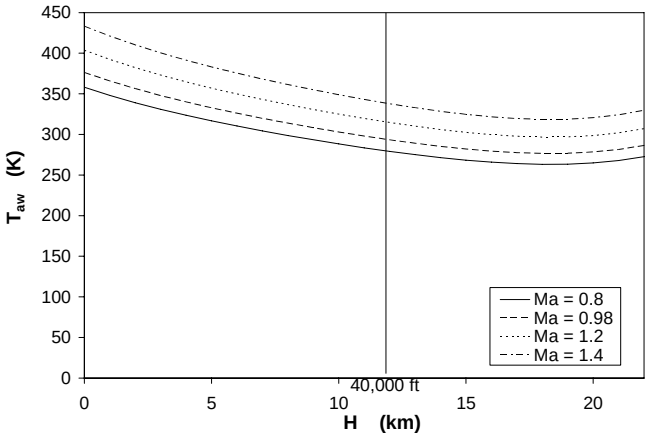


**Figure 8. Adiabatic wall temperature versus altitude for various Mach numbers (1% hot day).**

The overall trend of the adiabatic wall temperature with altitude follows the freestream air temperature in Figure 6. and increases with Mach number as expected. Figure 9 presents the temperature difference, $\Delta T = (T_{\mathrm{aw}}\text{-}T_\infty)$, versus altitude. This temperature difference demonstrates the increase in the adiabatic wall temperature over the freestream due to aerodynamic heating.

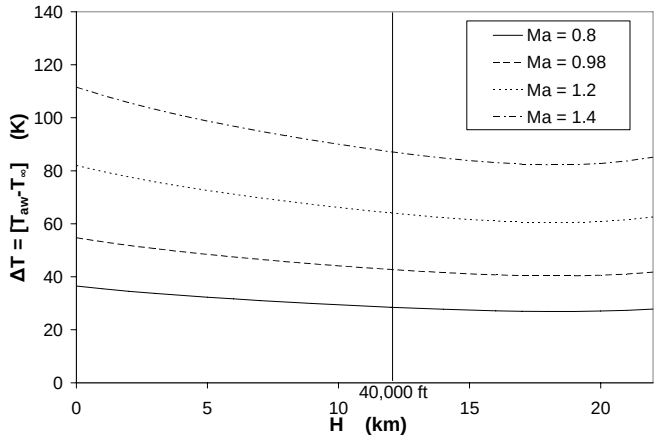


**Figure 9. Temperature difference $(T_{\mathrm{aw}} - T_\infty)$ versus altitude for various Mach numbers (1% hot day).**

The temperature difference $\Delta T = (T_{\mathrm{w}}\text{-}T_{\mathrm{aw}})$, a defining factor in heat flux, $q_w$", is given in Figure 10.

Of interest is the portion of the curves in which this difference is negative, which indicates that heat is transferred from the air to the aircraft skin. The maximum Mach number achievable before heat is transferred from the air to the skin is given by

$$\mathrm{Ma}_{\infty,\max} = \left[\frac{1}{r}\left(\frac{T_{\mathrm{w}}}{T_\infty} - 1\right)\left(\frac{2}{\gamma - 1}\right)\right]^{1/2} \tag{14}$$

and is plotted in Figure 11 over a range of wall temperatures.

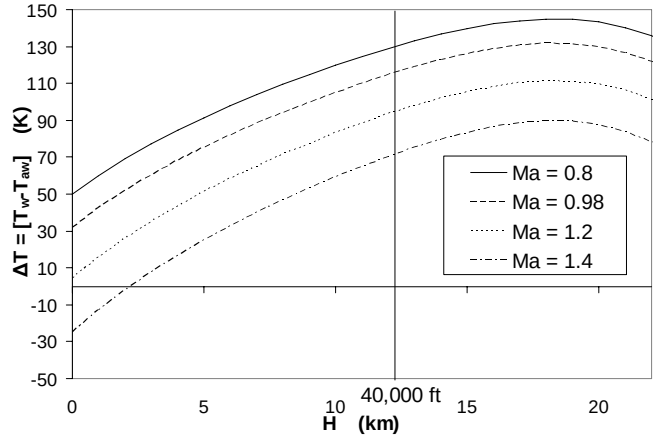


**Figure 10. Temperature difference $(T_{\mathrm{w}} - T_{\mathrm{aw}})$ versus altitude for various Mach numbers ($T_{\mathrm{w}}$ = 135ºC, 1% hot day).**

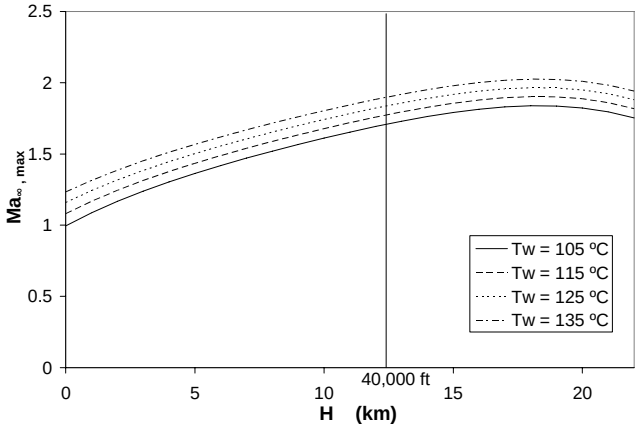


**Figure 11. Maximum Mach number before heat is transferred from the air to the skin versus altitude for various wall temperatures (1% hot day).**

The maximum Mach number increases with altitude and wall temperature. In Figure 12, the average convective heat transfer coefficient decreases monotonically with altitude due to the continual decrease in the air density. In general, the convective heat transfer coefficient increases with Mach number, as expected.

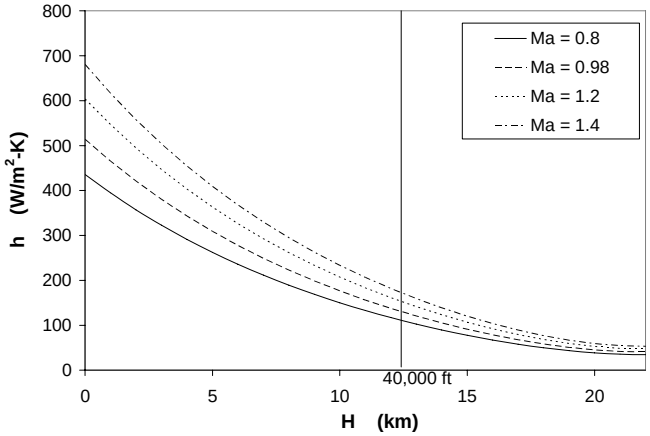


**Figure 12. Average convective heat transfer coefficient versus altitude for various Mach numbers ($T_w$ = 135ºC, $L$ = 1.0 m, 1% hot day).**

The average heat flux dissipated from the plate is shown in Figure 13. For low Mach numbers, the heat flux is positive for all values of altitude, which indicates that heat is transferred from the aircraft skin to the air.

At high Mach numbers, however, the heat flux is negative at low altitudes due to the negative $\Delta T$ as shown in Figure 10. This means that the adiabatic wall temperature is higher than the skin temperature due to aerodynamic heating effects. The effect of heated plate length on the average heat flux for $H$ = 0, 10, and 20 km is shown in Figure 14, Figure 15, and Figure 16. In general, the average heat flux decreases with plate length, and follows the behavior of the local heat transfer coefficient, where $h_L$ is high at the leading edge and decreases as the boundary layer grows.

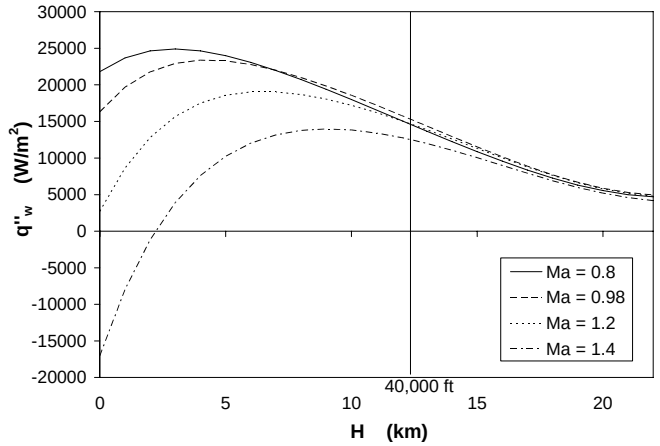


**Figure 13. Average heat flux dissipated over the plate versus altitude for various Mach numbers ($T_w$ = 135ºC, $L$ = 1.0 m, 1% hot day).**

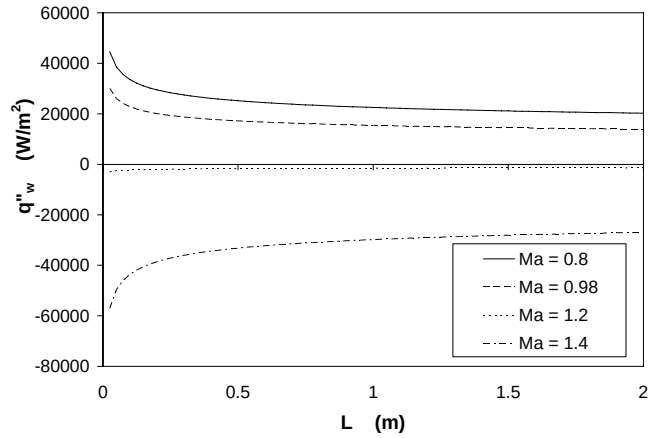


**Figure 14. Average heat flux dissipated over the plate versus plate length for various Mach numbers ($H$ = 0 km, $T_w$ = 135ºC, 1% hot day).**

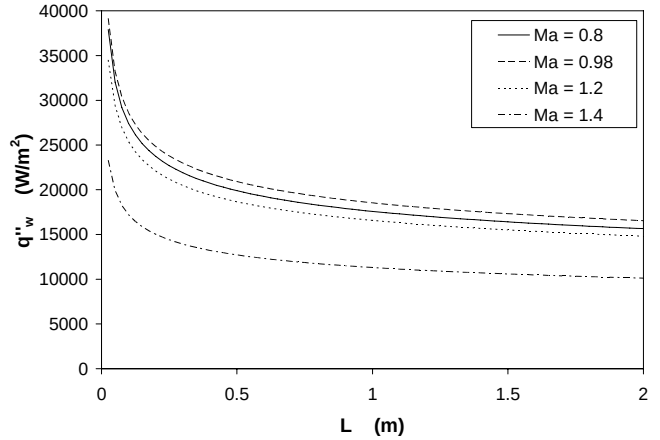


**Figure 15. Average heat flux dissipated over the plate versus plate length for various Mach numbers ($H$ = 10 km, $T_w$ = 135ºC, 1% hot day).**

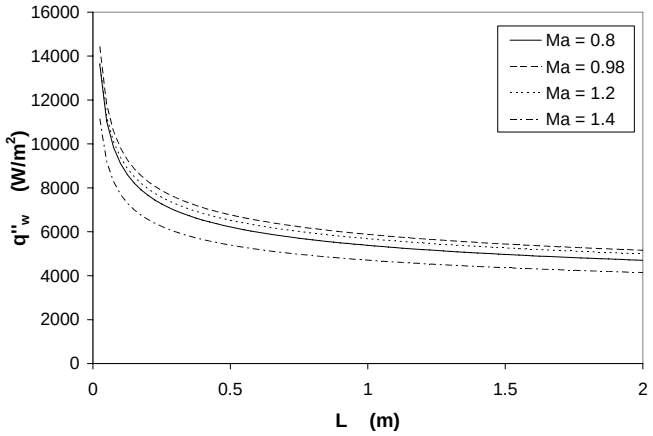


**Figure 16. Average heat flux dissipated over the plate versus plate length for various Mach numbers (*H* = 20 km, $T_w$ = 135ºC, 1% hot day).**

Figure 17 shows the average heat flux dissipated over the plate versus altitude for the 1% hot day, the 1% cold day, and the standard atmosphere data as presented in Figure 6 and Figure 7.

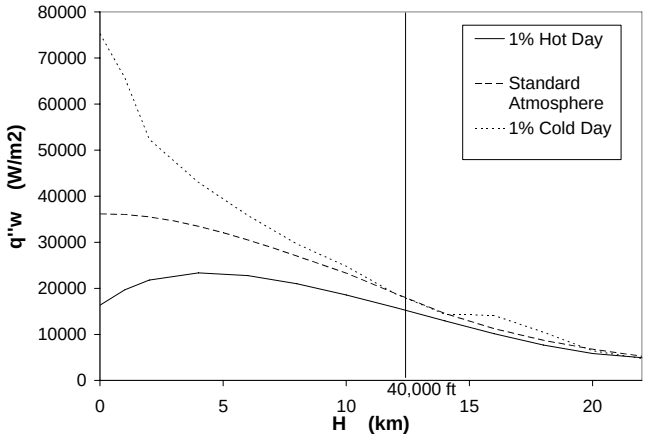


**Figure 17. Average heat flux dissipated over the plate versus altitude for various atmospheric conditions ($T_w$ = 135ºC, *L* = 1.0 m, $Ma_\infty$ = 0.98).**

At low altitudes, $q''_w$ is significantly higher for the 1% cold day due to the combined effects of the lower atmospheric temperature and the higher air density. The effect of wall temperature on average heat flux for a given airspeed is shown in Figure 18. The heat flux increases dramatically with altitude and wall temperature for low altitudes.

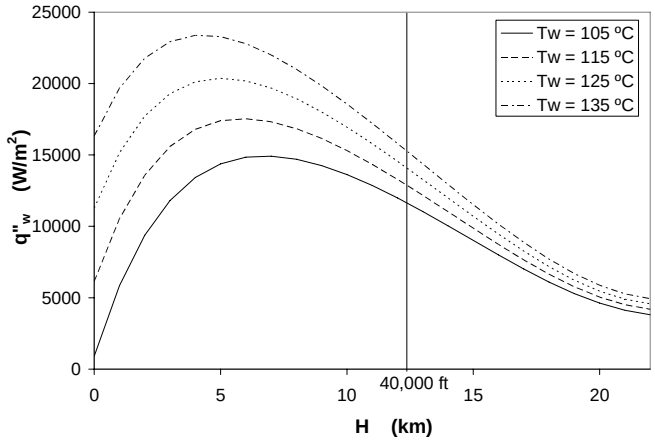


**Figure 18. Average heat flux dissipation versus altitude for various wall temperatures ($Ma_\infty$ = 0.98, *L* = 1.0 m, 1% hot day).**

An analysis of the heat transfer from a heated plate has provided important insights for the possible use of the aircraft skin to reject heat from electric actuator systems. It was found that the altitude and speed of the aircraft significantly affected the amount of heat that could be rejected from the skin. Aerodynamic heating of the skin reduced the heat transfer, and if the Mach number was high enough, heat transfer from the skin to the air went to zero. A performance map of this phenomenon was provided. The altitude of the aircraft affected the freestream temperature and density, which in turn affected the overall heat transfer coefficient. It was also shown that assumption of a "standard atmosphere" could result in significant errors in the prediction of the heat dissipation as compared to the data for the 1% hot day or the 1% cold day. Finally, the analysis showed that the aircraft skin temperature, which is directly influenced by the actuator thermal management system, has a strong effect on the heat dissipation rate, especially at low altitudes.

## CONCLUSION

A description of the experimental setup for a LHP subjected to steady state accelerations was presented. Experimentation will be conducted through the summer of 2006. A mathematical model of aerodynamic heating of a flat plate subjected to sub- and supersonic flow was also examined. It was found that for higher Mach numbers, heat is actually absorbed by the flat plate rather than rejected.

## ACKNOWLEDGMENTS

This research was conducted at the Air Force Research Laboratory, Propulsion Directorate, Power Division, Electrochemistry and Thermal Sciences Branch, AFRL/PRPS, Wright-Patterson Air Force Base, Ohio.

## REFERENCES


1. Quigley, R., "More Electric Aircraft," Proceedings of 1993 Applied Power Electronics Conference, 1993
2. Cloyd, J., "A Status of the United States Air Force's More Electric Aircraft Initiative," SAE Paper #97173, SAE Conference, Blacksburg, VA, 1997
3. Vrable, D., Yerkes. K., "A Thermal Management Concept for More Electric Aircraft Power System Applications," SAE Paper #981289, Aerospace Power Systems Conference Proceedings, Williamsburg, VA, 1998
4. Maidanik, F., et al., "Heat Transfer Apparatus," U.S. Patent 4515209, 1985.
5. Wirsch, P., "An Experimental and Numerical Investigation of a Stainless Steel/Ammonia Loop Heat Pipe," M.S. Thesis, Wright State University, Dayton, OH, 1995.
6. Ku, J., Ottenstein, L., Kaya, T., Rogers, P., Hoff, C., "Testings of a Loop Heat Pipe Subjected to Variable Accelerating Forces, Part 1: Start-up," SAE Paper #2000-01-2488, 2000
7. Ku, J., Ottenstein, L., Kaya, T., Rogers, P., Hoff, C., "Testings of a Loop Heat Pipe Subjected to Variable Accelerating Forces, Part 2: Temperature Stability," SAE Paper #2000-01-2489, 2000
8. Kaya, T., Ku, J., "Experimental Investigation of Performance Characteristics of Small Loop Heat Pipes," 41st Aerospace Sciences Meeting and Exhibit, Reno, Nevada, 2003.
9. DOD, Global Climatic Data for Developing Military Products, Department of Defense Handbook, MIL-HDBK-310, 1997.
10. Anderson, J., Introduction to Flight, Fourth edn., McGraw-Hill, Boston, 2000.
11. White, F., Heat and Mass Transfer, Addison-Wesley, New York, 1988.
12. NACA, Equations, Tables, and Charts for Compressible Flow, NACA Report 1135, U.S. Government Printing Office, Washington, D.C., 1953.
13. Incropera, F., DeWitt, D., Fundamentals of Heat and Mass Transfer, Third edn., Wiley, New York, 1990.


## NOMENCLATURE

| | |
|---|---|
| $a$ | Speed of sound, m/s; acceleration, m/s$^2$ |
| $A$ | Area, m$^2$ |
| $C^*_{f,L}$ | Local skin friction coefficient evaluated at the end of the plate |
| $c_p$ | Specific heat, J/(kg-K) |
| $g$ | Acceleration due to gravity, m/s$^2$ |
| $h_L$ | Local heat transfer coefficient at the end of the plate, W/(m$^2$-K) |
| $\bar{h}$ | Overall heat transfer coefficient, W/(m$^2$-K) |
| $H$ | Altitude, m |
| $k$ | Thermal conductivity, W/(m-K) |
| $L$ | Plate length, m |
| Ma | Mach number |
| Pr | Prandtl number |
| $q_x$ | Heat rate generated by the electronics package, W |
| $q''_w$ | Average heat flux dissipated from the plate, W/m$^2$ |
| $r$ | Recovery factor; radial coordinate, m |
| $R$ | Particular gas constant, m$^2$/(s$^2$-K), or thermal resistance, K/W |
| $Re_L$ | Reynolds number evaluated at the end of the plate |
| $St_L$ | Local Stanton number evaluated at the end of the plate |
| $t$ | Thickness, m |
| $T$ | Temperature, K |
| $T_{aw}$ | Adiabatic wall temperature, K |
| $T_w$ | Wall temperature, K |
| $U$ | Velocity, m/s |
| $V$ | Voltage, V |
| γ | Ratio of specific heats |
| $\Delta T$ | Temperature difference, K |
| $\mu$ | Absolute viscosity, (N-s)/m$^2$ |
| $\rho$ | Density, kg/m$^3$ |

*Superscripts*

| | |
|---|---|
| * | Film condition |
| + | Normalized |

*Subscripts*

| | |
|---|---|
| ∞ | Freestream condition |
| aw | Adiabatic wall |
| ct | Centrifuge table |
| hs | Heat spreader |
| max | Maximum value |
| R | Reference condition |
| w | Aircraft skin |